Accounting for rotation in a multi-stage cyclo-symmetric model - a case study

E. Balmes [1,2], **I. Bucher**[3]
[1] SDTools [2] Arts et Metiers ParisTech [3] Technion

Abstract
Rotating structures typically have stages with cyclo-symmetric geometries that are periodic by rotation. The spatial Fourier transform of fields at periodic positions leads to multiple uncoupled low cost problems for each Fourier harmonic. Real rotors are assemblies of stages that have different number of sectors. This motivated the extension of cyclo-symmetry to multistage assemblies. The resulting methodology gives access to low cost predictions of full rotor dynamics. The present paper summarizes the theory and shows that this new ability is useful to analyze gyroscopic and centrifugal softening effects in detail for configurations where beam mass model are traditionally used.

1 Introduction

Rotating structures typically have stages with cyclo-symmetric geometries. Classically cyclic-symmetry [1, 2] considers single stage vibration or assumes the whole rotor to have a single number of sectors. But real rotors are assemblies of stages that have different angular periodicity. This has motivated the extension of cyclo-symmetry to multistage assemblies for mono-harmonic solutions [3] and full system models [4, 5].

After an introduction of the cyclic symmetry and its extension to multi-stage configurations, the paper summarizes the reduction strategy [6] used to approximate responses at variable rotation speeds using a limited number of full model evaluations. The proposed methodology is then used on the case of a rotor consisting of a heavy impeller with 8 sectors and a turbine with 40 blades. The disks are modeled using detailed volume element meshes, which are typically needed for accurate stress predictions. The full 3D model with 5 million DOF is too large for convenient numerical predictions of global dynamics. The multi-stage cyclic symmetry implemented in the SDT/Rotor toolbox [7] running in the Matlab environment is used to correlate free-free modes of the rotor and predict Campbell diagrams, where the difference between beam and 3D models are clearly apparent.

2 Theory

Section 2.1 first introduces classical cyclic symmetry through spatial Fourier transform basics. Following the presentation in [5], case of multi-stage models is treated trough separate transforms of each stage and coupling by inter-stage stiffness. The second aspect of the paper is the use of these models to predict full rotor dynamics. Equations associated with classical effects, gyroscopic coupling, centrifugal softening, ... are given in section 2.3, and the use of fixed basis reductions to predict rotation dependent responses is finally presented.

2.1 Cyclic symmetry

Points of a structure with a cyclo-symmetric geometry can be grouped in series of NS (number of sectors) points $\mathbf{x}^s$ whose location is given by a simple rotation of a nominal sector. Taking any field v, one defines a vector $\{\mathbf{v}\}_{NS}$ that contains all the terms in the spatial series $(\mathbf{v}(\mathbf{x}^s))$ and a transformed vector $\{\widehat{\mathbf{v}}\}_{NS}$ that contains all the Fourier harmonics

$$\begin{array}{rcl} \{\mathbf{v}\}^\top & = & \left\{ \begin{array}{ccccccc} \mathbf{v}(\mathbf{x}^0) & \cdots & \mathbf{v}(\mathbf{x}^s) & \cdots & \mathbf{v}(\mathbf{x}^{N_s-1}) \end{array} \right\}, \\ \{\widehat{\mathbf{v}}\}^\top & = & \left\{ \begin{array}{ccccccc} \widehat{\mathbf{v}}_0(\mathbf{x}^0) & \cdots & \Re\left(\widehat{\mathbf{v}}_\delta(\mathbf{x}^0)\right) & \Im\left(\widehat{\mathbf{v}}_\delta(\mathbf{x}^0)\right) & \cdots & \widehat{\mathbf{v}}_{\frac{N_s}{2}}(\mathbf{x}^0) \end{array} \right\}. \end{array} \tag{1}$$

these two vectors are related by the unitary discrete Fourier transform

$$\{\widehat{\mathbf{v}}\} = \left[E^{-1}\right]\{\mathbf{v}\}, \tag{2}$$

and its inverse

$$\{\mathbf{v}\} = [E]\{\widehat{\mathbf{v}}\}. \tag{3}$$

where the Fourier transform is here specified as matrix $[E]$

$$[E] = \frac{1}{\sqrt{N_s}} \begin{bmatrix} 1 & \cdots & \sqrt{2} & 0 & \cdots & 1 \\ \vdots & & \vdots & \vdots & & \vdots \\ 1 & \cdots & \sqrt{2}\cos(s\,\delta\,\alpha) & -\sqrt{2}\sin(s\,\delta\,\alpha) & \cdots & (-1)^s \\ \vdots & & \vdots & \vdots & & \vdots \\ 1 & \cdots & \sqrt{2}\cos((N_s-1)\,\delta\,\alpha) & -\sqrt{2}\sin((N_s-1)\,\delta\,\alpha) & \cdots & (-1)^{N_s-1} \end{bmatrix} \tag{4}$$

When considering a full 3D model, matching DOFs in each sector can be arranged as vectors $\{\mathbf{v}\}$ and transformed separately. This transformation generates two harmonic DOF vectors $\{\widehat{q}\}$ and $\{\widehat{f}\}$ that are the transforms of full DOF vectors $\{q\}$ and $\{f\}$ respectively. The sector number in spatial space is thus replace by harmonic number in wave-number space. The Fourier harmonic index δ happens to correspond to the number of times a given field changes sign over a half circle, so that the classical denomination for δ is *diameter number*.

Assuming that the properties of each sector are identical (the case of mistuned disks is discussed in [5]), one can show that the transform of the system equations $[Z]\{q\} = \{f\}$ takes the block form

$$\begin{bmatrix} Z^0 & \cdots & 0 & 0 & \cdots & 0 \\ \vdots & \ddots & \vdots & \vdots & & \vdots \\ 0 & \cdots & Z^0 & 0 & \cdots & 0 \\ 0 & \cdots & 0 & Z^0 & \cdots & 0 \\ \vdots & & \vdots & \vdots & \ddots & \vdots \\ 0 & \cdots & 0 & 0 & \cdots & Z^0 \end{bmatrix} \begin{Bmatrix} \widehat{q}_0 \\ \vdots \\ \Re\left(\widehat{q}_\delta\right) \\ \Im\left(\widehat{q}_\delta\right) \\ \vdots \\ \widehat{q}_{\frac{N_s}{2}} \end{Bmatrix} = \begin{Bmatrix} \widehat{f}_0 \\ \vdots \\ \Re(\widehat{f}_\delta) \\ \Im(\widehat{f}_\delta) \\ \vdots \\ \widehat{f}_{\frac{N_s}{2}} \end{Bmatrix}. \tag{5}$$

The block form is valid for purely disjoint sectors, in reality sectors are connected by edges and the motion on the left edge of one sector is equal to the motion on the right edge of the previous sector. The inter-sector continuity constraint does not couple Fourier harmonics so that the full model (5) can be decomposed in a series of independent problems associated with each harmonic (classically called diameter) :

- for $\delta = 0$, $\{\widehat{q}_0\}$ is real and satisfies

$$\begin{array}{rcl} \left[Z^0\right]\{\widehat{q}_0\} & = & \{\widehat{f}_0\}, \\ \left[c_l - c_r\right]\{\widehat{q}_0\} & = & \{0\}. \end{array} \tag{6}$$

  where c_l, c_r are observation equations relating the motion on edges to the full set of DOFs in the sector. For 3D fields such as displacement, the components are projected on a basis local to the edge with a rotation angle corresponding to the number of sectors.

- if $\delta \neq 0$ and $\delta \neq N_s/2$, $\{\widehat{q}_\delta\}$ is complex and satisfies

$$\begin{aligned} \begin{bmatrix} Z^0 & 0 \\ 0 & Z^0 \end{bmatrix} \begin{Bmatrix} \Re\left(\widehat{q}_\delta\right) \\ \Im\left(\widehat{q}_\delta\right) \end{Bmatrix} &= \begin{Bmatrix} \Re(\widehat{f}_\delta) \\ \Im(\widehat{f}_\delta) \end{Bmatrix}, \\ \begin{bmatrix} c_l - c_r\,\cos(\delta\,\alpha) & c_r\,\sin(\delta\,\alpha) \\ -c_r\,\sin(\delta\,\alpha) & c_l - c_r\,\cos(\delta\,\alpha) \end{bmatrix} \begin{Bmatrix} \Re\left(\widehat{q}_\delta\right) \\ \Im\left(\widehat{q}_\delta\right) \end{Bmatrix} &= \begin{Bmatrix} 0 \\ 0 \end{Bmatrix}. \end{aligned} \tag{7}$$

- if $\delta = N_s/2$, $\{\widehat{q}_{\frac{N_s}{2}}\}$ is real and satisfies

$$\begin{aligned} [Z^0] \left\{\widehat{q}_{\frac{N_s}{2}}\right\} &= \{\widehat{f}_{\frac{N_s}{2}}\}, \\ [c_l + c_r] \left\{\widehat{q}_{\frac{N_s}{2}}\right\} &= \{0\}. \end{aligned} \tag{8}$$

When all the individual responses have been computed, the full response is obtained by Fourier synthesis thanks to (3).

2.2 Multi-stage cyclic symmetry

For multi-stage cyclic symmetry, the stages each have their own spatial periodicity. Assuming that stages are disjoint, the Fourier transform can be applied to each separately, leading to two problems of form (5).

The inter-stage coupling is achieved by a dynamic stiffness $\left[\widehat{Z}_\delta^{\mathcal{R}}\right]$ that is meshed using physical elements shown in red in figure 1. The requirement [5] to use standard elements that are not too distorted, while leading to well posed problems, can be difficult if the disk meshes have very different refinements (see figure 4). It is thus proposed here to achieve coupling by computing the energy of a penalized representation of bilateral contact between surfaces of the two disks.

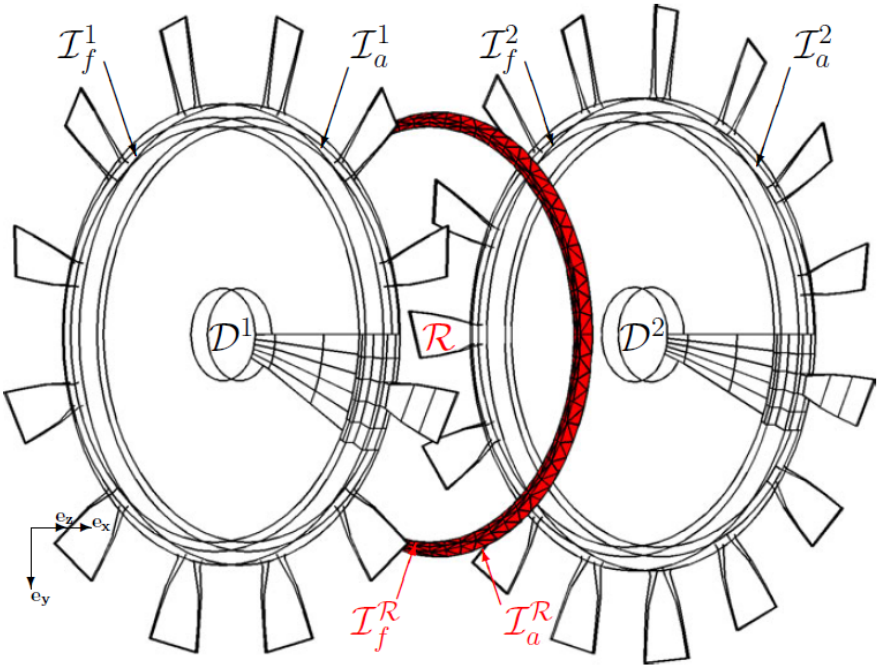

Figure 1: Sample mesh of a 2 disk application.

As argued in Refs [3, 5], one can, for low diameter numbers, assume that shaft modes a composed of a single Fourier harmonic. In cases with complex Fourier harmonics ($\delta \neq 0\,[\mathrm{lcm}(N_s^1, N_s^2)]$ and $\delta \neq 0\,[N_s^1/2]$ and

$\delta \neq 0\,[N_s^2/2]$), the solutions satisfy system equations for the real and imaginary components of the response of each stage, coupled by the inter-stage stiffness $\left[\widehat{Z}_\delta^{\mathcal{R}}\right]$ and the inter-sector continuity conditions verified independently by each stage

$$\begin{aligned}
&\left(\begin{bmatrix} Z^{1,0} & 0 & 0 & 0 \\ 0 & Z^{1,0} & 0 & 0 \\ 0 & 0 & Z^{2,0} & 0 \\ 0 & 0 & 0 & Z^{2,0} \end{bmatrix} + \left[\widehat{Z}_\delta^{\mathcal{R}}\right]\right) \begin{Bmatrix} \Re(\widehat{q}_\delta^1) \\ \Im(\widehat{q}_\delta^1) \\ \Re(\widehat{q}_\delta^2) \\ \Im(\widehat{q}_\delta^2) \end{Bmatrix} = \begin{Bmatrix} \Re(\widehat{f}_\delta^1) \\ \Im(\widehat{f}_\delta^1) \\ \Re(\widehat{f}_\delta^2) \\ \Im(\widehat{f}_\delta^2) \end{Bmatrix}, \\
&\begin{bmatrix} c_l^1 - \cos(\delta\,\alpha^1)\,c_r^1 & \sin(\delta\,\alpha^1)\,c_r^1 & 0 & 0 \\ -\sin(\delta\,\alpha^1)\,c_r^1 & c_l^1 - \cos(\delta\,\alpha^1)\,c_r^1 & 0 & 0 \\ 0 & 0 & c_l^2 - \cos(\delta\,\alpha^2)\,c_r^2 & \sin(\delta\,\alpha^2)\,c_r^2 \\ 0 & 0 & -\sin(\delta\,\alpha^2)\,c_r^2 & c_l^2 - \cos(\delta\,\alpha^2)\,c_r^2 \end{bmatrix} \begin{Bmatrix} \Re(\widehat{q}_\delta^1) \\ \Im(\widehat{q}_\delta^1) \\ \Re(\widehat{q}_\delta^2) \\ \Im(\widehat{q}_\delta^2) \end{Bmatrix} = \{0\}.
\end{aligned} \tag{9}$$

Similar equations are derived for cases with real harmonics of one or multiple stages.

The use of mono-harmonic modes to build a shaft model with sector having distinct periodicity will be illustrated here. The key extension in Ref [5] is the use of a few mono-harmonic modes to build reduced sector models that allow predictions of all the modes in the system.

When compared to full 3D simulations, cyclic symmetry uses the assumption of mono-harmonic responses to go from one full 3D problem to multiple one sector solutions. Solving multiple small problems is typically significantly cheaper than addressing the full system predictions. Post processing however requires the use of the Fourier transform (3), which can be something of a difficulty when the full 3D model contains millions of nodes.

In multi-stage analysis, harmonic decoupling is only approximate. In particular, aliasing occurs for diameters above the lowest half spectrum of a given stage. For the application shown here, one however focuses on 1 diameter modes associated with shaft bending and assuming mono-harmonic responses is very accurate.

2.3 Accounting for rotation effects

Since the geometry is not invariant by rotation, analysis of the rotating system must be performed in the body fixed frame. Matrices associated with motion in a non Galilean frame are well known (see [8, 9] for example) and given by

- $[M] = \int_{\mathcal{S}_0} \rho_0 [N_{xyz}]^\top [I] [N_{xyz}]\, d\mathcal{S}_0$ the mass in the rotating frame
- $[D_g] = \int_{\mathcal{S}_0} 2\rho_0 [N_{xyz}]^\top [\Omega] [N_{xyz}]\, d\mathcal{S}_0$ the gyroscopic coupling
- $[K_c] = \int_{\mathcal{S}_0} \rho_0 [N_{xyz}]^\top [\Omega^2] [N_{xyz}]\, d\mathcal{S}_0$ the spin softening
- $[K_a] = \int_{\mathcal{S}_0} \rho_0 [N_{xyz}]^\top \frac{\partial [\Omega]}{\partial t} [N_{xyz}]\, d\mathcal{S}_0$ the centrifugal acceleration
- $f_c = \int_{\mathcal{S}_0} \rho_0 [N_{xyz}]^\top [\Omega^2] \{p\}\, d\mathcal{S}_0$ the centrifugal load
- $f_g = \int_{\mathcal{S}_0} \rho_0 [N_{xyz}]^\top \frac{\partial [\Omega]}{\partial t} \{p\}\, d\mathcal{S}_0$ the Coriolis load

Coupling with the elastic K_e and geometric stiffening K_{geom} matrices, obtains system equations

$$[M]\{\ddot{q}\} + ([C + D_g(\Omega)])\{\dot{q}\} + \Big[K_e + K_{geom} + K_a(\dot{\Omega}) + K_c(\Omega)\Big]\{q\} = f_{ext} - f_c(\Omega) - f_g(\dot{\Omega}) \tag{10}$$

In the applications considered in this study, one will use a fixed axis of rotation $\Omega = \omega(t)\{e_z\}\wedge$. The matrices and loads are thus proportional to the scalars ω, ω^2 and $\dot{\omega}$ and one can use

$$[D_g(\omega)] = \omega [D_g(1)]$$

which results in significant computational cost savings since the matrix only needs to be computed for a single velocity. One proceeds similarly for the other matrices and loads.

Computations of interest are the *Campbell diagrams* where one seeks, as a function of rotation speed, the modes $\{\psi_j\}$ and poles λ_j verifying the eigenvalue problem

$$\Big[[M]\lambda_j^2 + ([C + D_g(\Omega)])\lambda_j + [K_e + K_{geom} + K_c(\Omega)]\Big]\{\psi_j\} = 0 \tag{11}$$

When considering undamped rotors on isotropic bearings, the eigenvalues are real but modeshapes complex. Specific transformation [10] can be applied to obtain real modes and combining such transformation with cyclic symmetry seems possible by accounting for the phase shift of the mode pair found for non zero diameter modes. The application is however not trivial and the interest limited since the procedure does not apply to damped rotors. The reduction procedure proposed in section 2.4 also strongly diminishes the cost of using complex modes, so that they are used here.

To apply cyclic symmetry, the spatial Fourier transform (2) must thus be applied to the real and imaginary parts of the complex mode shape separately. The numerical implementation must thus choose between using complex numbers to represent the real and imaginary part of the spatial transform or those of the complex field. But other than this software difficulty the process is straight-forward.

Many excitations, imbalance, torque variation, aerodynamic pressure field, are at multiples of the rotation speed. One is thus interested in computing critical speeds where one neglects damping ($C = 0$) and assumes the modal frequency to be equal to a multiple of the rotation speed (in rev/s), that is $\lambda_j = ni\Omega$, thus leading to

$$\Big[-\Omega_j^2[M] + ni\Omega^2[D_g(1)] + [K_e + K_{geom}] + n^2\Omega^2 K_c(1)\Big]\{\psi_j\} = 0 \tag{12}$$

2.4 Model reduction for variable speed computations

While cyclic symmetry makes full rotor predictions accessible, computing the response of a range of speeds can however be quite costly. A solution, first proposed in [6], is to build a fixed Ritz basis to approximate solutions at variable speeds.

One thus builds a collection of vectors by assembling multiple modal bases

$$\Big[\hat{T}\Big] = [\phi_{1:NM}(\Omega_1) \; ... \; \phi_{1:NM}(\Omega_{Nw})] \tag{13}$$

with NM modes at NW rotation speeds. The vectors thus generated are not independent, so that a numerical procedure to generate a basis T of the subspace generated by $\hat{T}$ is used. Classical procedures [5] are Gramm-Schmidt, singular value decomposition and the orthogonal maximum sequence [11]. Once a basis generated each of the matrices and loads in (10)-(12) can be reduced using $T^T M T$, $T^T f$, ...

While using a fixed basis built using just a few velocities is an approximation, the results are quite sufficient to estimate the response over a large range of rotation speeds. The main development for this paper was to implement the combination of cyclic symmetry and this multi-speed modal basis approach for models including gyroscopic coupling and centrifugal softening.

3 A simple reference case

As a sample case, one will consider a volume model of the rotor studied in Ref.[12]. As shown in figure 2, the first bending mode has a strong frequency split due to gyroscopic effects and a critical speed around 3159

RPM. At this frequency centrifugal softening makes the stiffness contribution singular, that is $[K_e + \Omega^2(K_c(1) + iD_g(1))]\{\psi\} = 0$ has a solution and in body fixed coordinates the whirl direction changes.

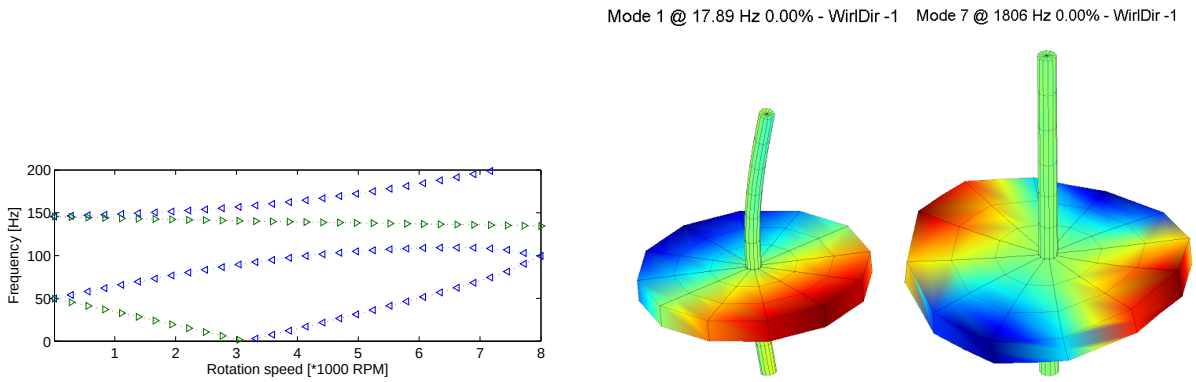

Figure 2: Left: Campbell diagram in body fixed coordinates. Triangles pointing right indicate forward whirl. Center: backward whirl associated with first bending mode. Right : backward whirl mode associated with 2 diameter bending of the disk.

As this simple 3D model only contains 2367 DOF, one could verify that solutions computed using cyclic symmetry gave the same results as the full 3D with relative errors on frequencies below 1e-6. The advantages of cyclic symmetry are faster solutions and better numerical conditioning.

The next verification is a check that gyroscopic and centrifugal softening effects can be well predicted in the basis of nominal elastic modes. As shown in figure 3, the error associated with a computation based on the first bending mode only is below 6.5%. For the first disk bending, which has two diameters and a low split due to gyroscopic effects, the relative error on frequency associated with a single mode computation is below 1e-4.

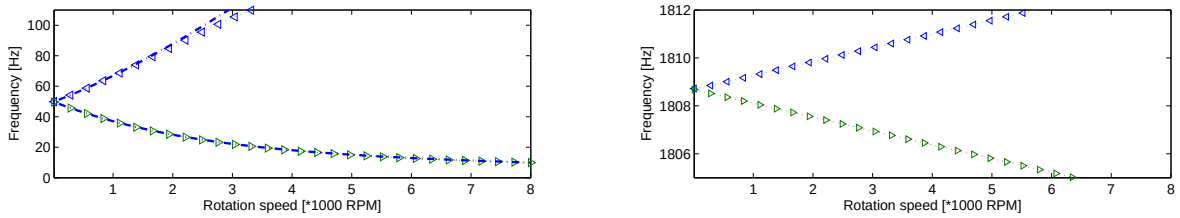

Figure 3: Campbell diagrams. Left: computed with 1 mode or exactly. Right: first disk bending mode.

4 A realistic application

4.1 Model and free/modes

The rotor considered in this section consists of a slender shaft, a turbine and a large and heavy impeller. The operating speed is 50,000 RPM. The ANSYS study begun by running an automatic meshing process using ANSYS workbench. The result is shown in figure 4. The fine mesh generated by ANSYS contains approximately 5 million DOF. For such a complex body, only non rotating analysis was performed.

A model with two base sectors was imported in to SDT. The impeller (on the left in dark red) is meshed in 8 sectors using 41,736 elements and 69,440 nodes. The turbine is composed of a disk and 45 blade. The

turbine and shaft are modeled using 45 sectors and use 18,257 second order volume elements and 41,213 nodes. Accounting for nodes common at interfaces, the full 3D model would have 2 million nodes (6e6 DOF) and 1,155,453 elements. This mesh, with second order elements, represents model that is very expensive to evaluate.

Accounting for cyclic symmetry, one only has 307428 DOF for zero diameter modes, and twice that number for higher diameters that number doubles. Computation of 30 modes takes around 300 s with SDT/Rotor [7], which is a major speedup compared to the full model computation.

The zoom on the shaft / impeller area shows that significantly different mesh densities were used on the two components. Meshing the connection area, as proposed in [5], is thus impractical and a penalized contact strategy was implemented.

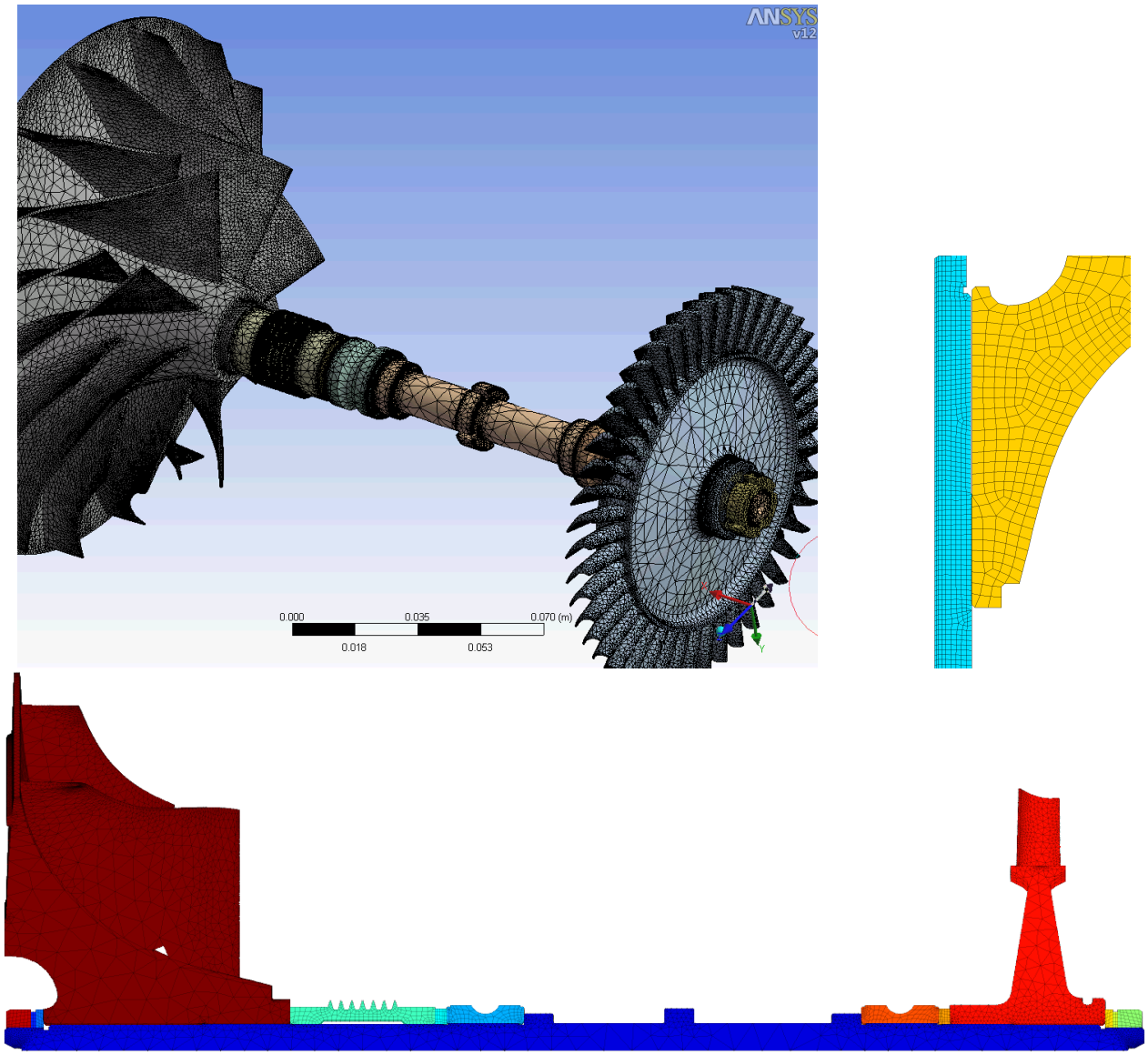

Figure 4: Top: Sample rotor meshed in ANSYS. Top right : mesh section at the impeller shaft interface. Bottom: sector model imported into SDT.

As shown in figure 5, an experimental modal test was performed in free/free boundary conditions leading to responses and modal frequencies shown in table 1. Computed modes shown in figure 6 correlate fairly well even though the test has lower frequencies. The exact geometry and properties of the labyrinth is not

Table 1: Free/free modes of the rotor.

Name	ANSYS Full	SDT cyclic	Beam model	Measured
	Hz	Hz	Hz	Hz,%
First bending	528.53	514.3	462	460 1.6%
Torsion	588.2	567.3		
Second bending	1724	1586	1270	1405 2.6%
Global bending	3452	2952	2876	1866 1.6%

very clear and this area has a significant impact on frequencies. A refined modal test would however be needed to confirm the exact modifications needed in particular to predict the global bending at 1866 Hz. The correlation was thus deemed acceptable as is.

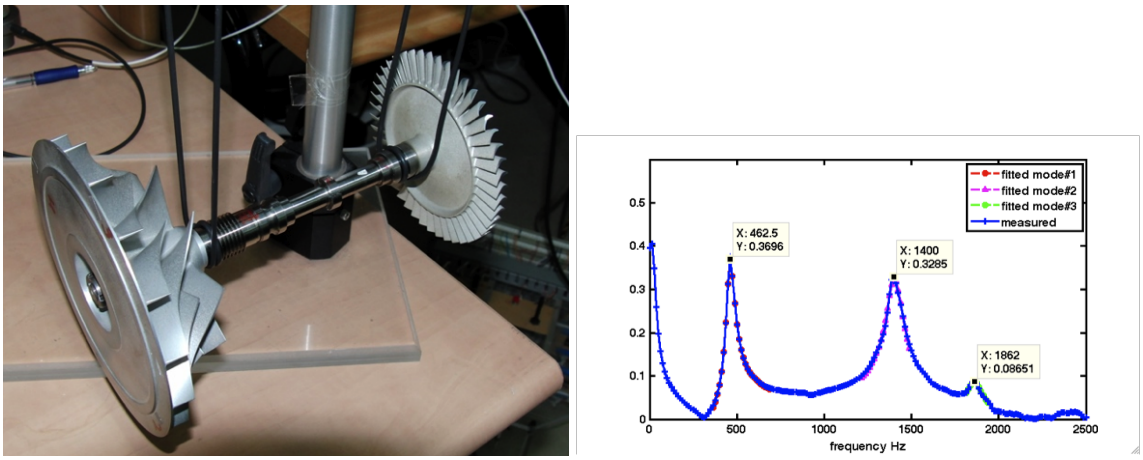

Figure 5: Free/free test of the rotor modes of the rotor.

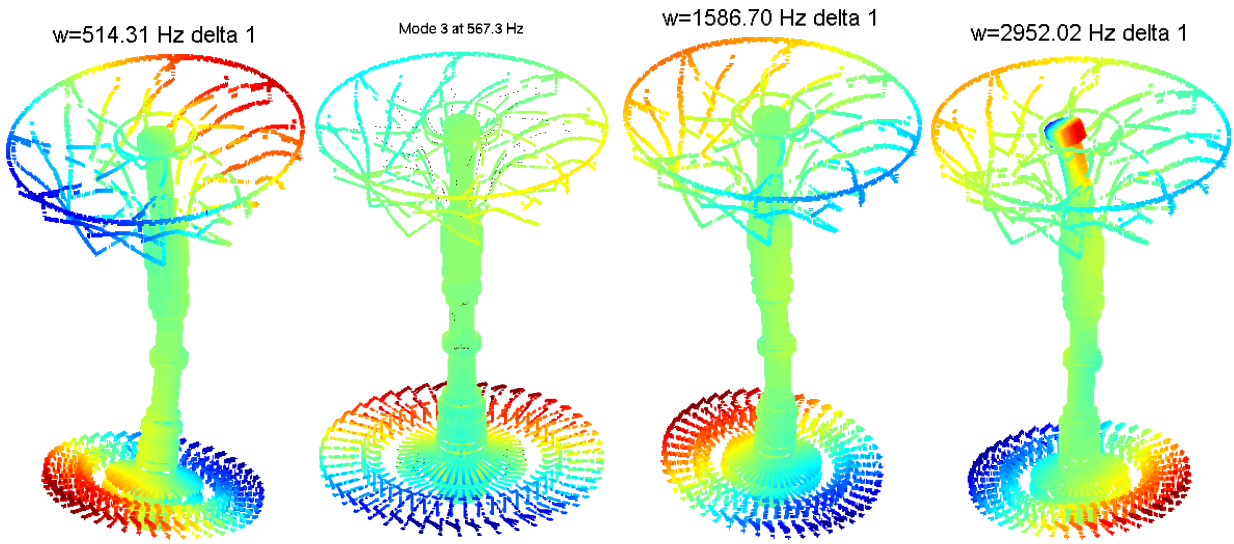

Figure 6: Free/free modes of the rotor. Multistage cyclic symmetry in SDT. Color is x motion for torsion and z otherwise.

Inspecting the results, it was observed that the discs show little distortion in the operating range of 0-50,000 RPM. Replacing blades by disc-like elements thus seems appropriate. A simple Matlab-based Timoshenko-beam rotor-dynamics code that incorporates effects of rotation [13] was used for comparison. The first two elastic modes are shown in figure 7. Improved frequency match was obtained by slightly modifying elements and material constants around regions with the largest bending stress.

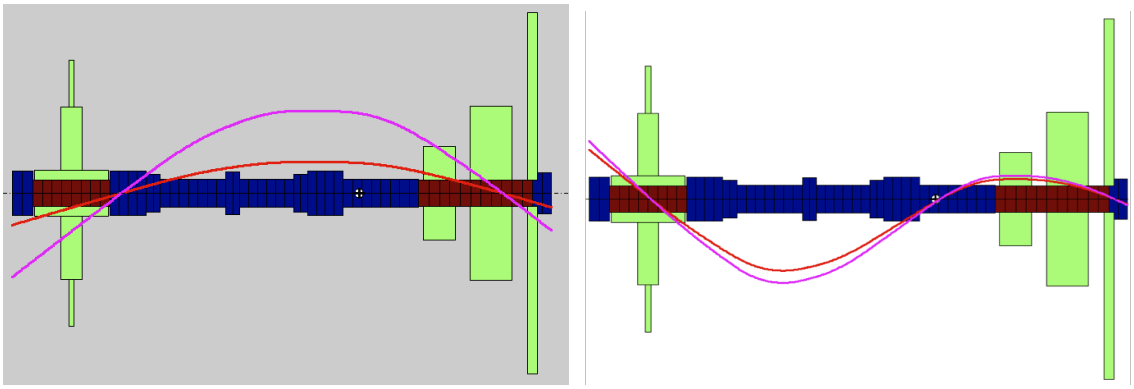

Figure 7: Free/free modes of the non rotating beam model. 461 and 1270 Hz

4.2 Predictions of rotating response

In order to examine the behavior of the system under realistic conditions, simple self-aligning ball-bearings were added to the beam model to realize a simply supported rotating shaft. Modes of interest are now the first global bending with nodes near the bearings, a turbine bending mode near 980 Hz and an impeller bending at 1924 Hz.

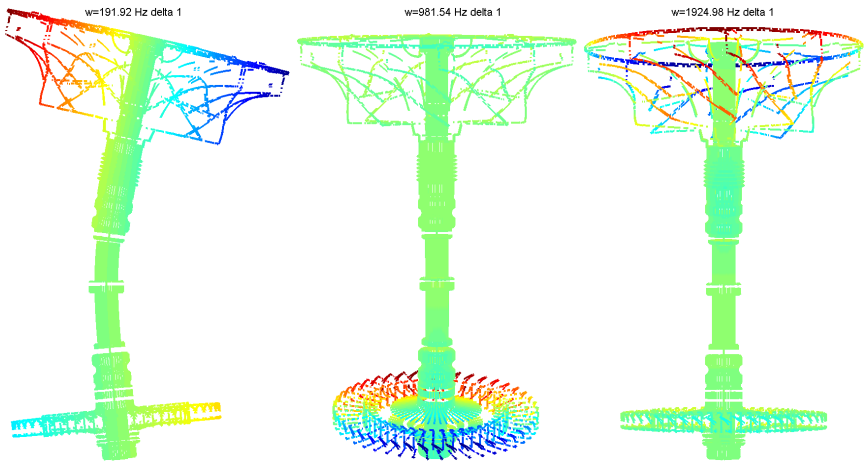

Figure 8: Campbell diagram predicted with beam (left) and 3D model (right).

Figure 9 compares the Campbell diagrams obtained with the beam and the 3D cyclic symmetry models. For 3D prediction, frequencies are shifted to account for the fact that predictions are performed in the body fixed frame.

The effect of rotation is clearly visible. A number of critical frequencies are indicated as circles in the diagram of the beam model. The critical frequencies associated with forward whirl modes (indicated as solid circles) are typically excited by imbalance [12] and thus important to analyze. The same two critical speeds

are found in the 3D diagram. The disk flexibility however plays a major role inducing significant shift of the second critical speed.

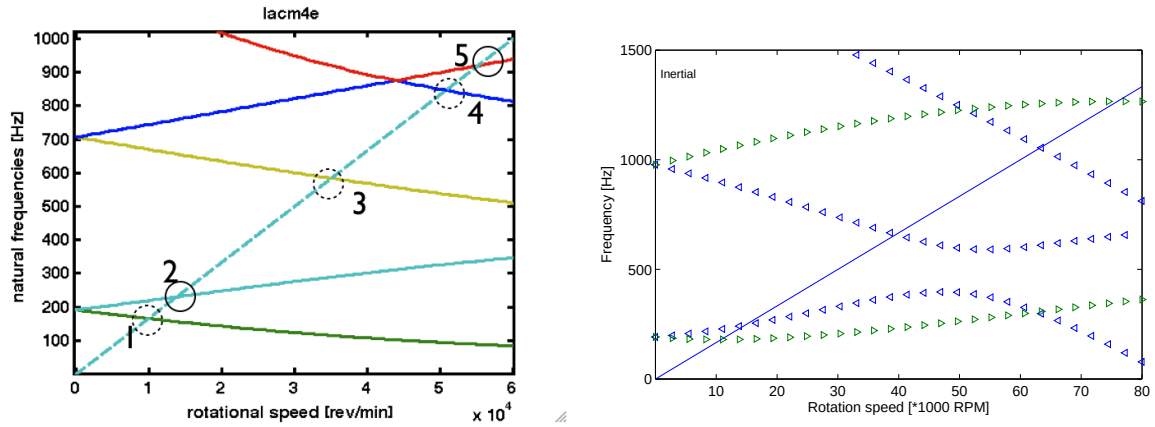

Figure 9: Campbell diagram predicted with beam (left) and 3D model (right). Circles indicated critical speeds for forward (solid) and backward (dotted) modes.

Visualizing modeshapes at critical speeds is an important design tool. The first critical speed corresponds to global bending of the shaft. At the second critical speed (circle number 5), both the beam and 3D models (right) show a localization of the mode on the turbine. The shaft area near the turbine was however identified as important for the free-free mode correlation so that further validation of the shaft model is important here.

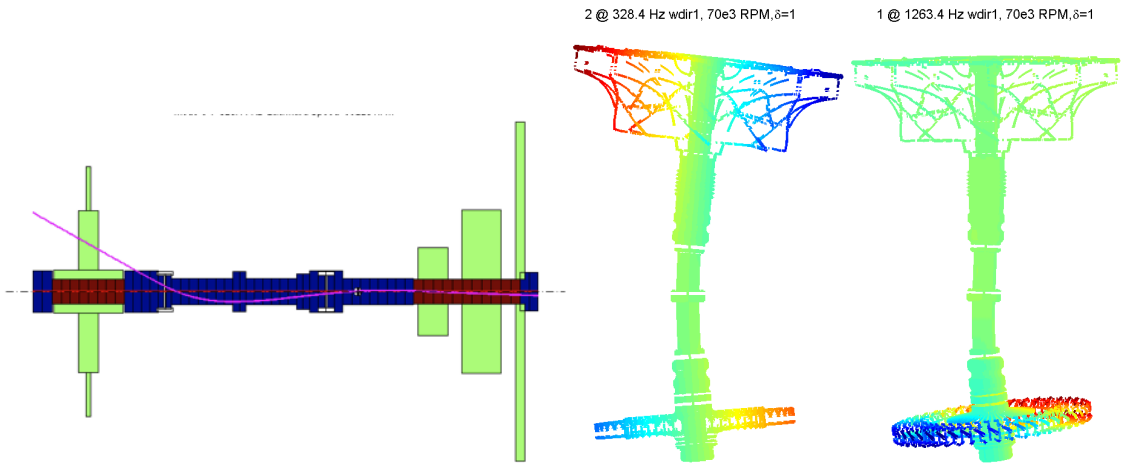

Figure 10: Forward critical modes. Left : beam mode 2 (left), volume modes 1 (center) 2 (right)

5 Conclusion

The use of cyclic symmetry and fixed basis parametric models makes the prediction of responses as a function of rotation speed accessible for full 3D models.

The classical approach based on beam and rigid disk models is a rather elaborate process that requires many adjustments and significant expertise to properly define disks, in particular when representing heavy impellers such as the one considered in the application. This strategy is however well mastered in industry and the proposed methods are well suited to replace beam models by volume elements, which have the clear

advantage of allowing studies of disk flexibility. For a volume model with the geometry of the beam model shown earlier, computation of a Campbell diagram runs in a few CPU seconds, so that cyclic symmetry models are directly competitive with beam models.

Multi-stage cyclic symmetry gives access to the actual shaft geometry. In the present application, complete analysis ran in less than 10 mn. While this may be too slow for parametric optimization procedures, the accuracy associated with proper accounting of the local flexibilities is definitely an advantage in validation phases.

References

[1] **Thomas, D.**, *Dynamics of rotationally periodic structures*, International Journal for Numerical Methods in Engineering, Vol. 14, pp. 81–102, 1979.

[2] **Wildheim, J.**, *Excitation of rotationally circumferentially periodic structures*, Journal of Sound and Vibration, Vol. 75, No. 3, pp. 397–416, 1981.

[3] **Laxalde, D., Lombard, J.-P.** and **Thouverez, F.**, *Dynamics of Multistage Bladed Disks Systems*, ASME Journal of Engineering for Gas Turbines and Power, Vol. 129, pp. 1058–1064, 2007.

[4] **Sternchüss, A. and Balmes, E.**, *Reduction of Multistage disk models : application to an industrial rotor*, *Proceedings of GT2008, ASME Turbo Expo*, 2008, paper Number GT2008-50580.

[5] **Sternchüss, A.**, Multi-level parametric reduced models of rotating bladed disk assemblies, Ph.D. thesis, Ecole Centrale de Paris, 2009.

[6] **Sternchüss, A.** and **Balmes, E.**, *On the reduction of quasi-cyclic disks with variable rotation speeds*, *Proceedings of the International Conference on Advanced Acoustics and Vibration Engineering (ISMA)*, pp. 3925–3939, 2006.

[7] **Balmes, E.** and **Bianchi, J.**, Rotor module for SDT, User Manual, SDTools, 2008-2009.

[8] **Desceliers, C.**, Dynamique non linéaire en déplacements finis des structures tridimensionnelles viscoélastiques en rotation, Ph.D. thesis, École Centrale de Paris, 2001.

[9] **Géradin, M.** and **Rixen, D.**, Mechanical Vibrations. Theory and Application to Structural Dynamics., John Wiley & Wiley and Sons, 1994, also in French, Masson, Paris, 1993.

[10] **Wang, W.** and **Kirkhope, J.**, *New eigensolutions and modal analysis for gyroscopic rotor systems, part 1 undamped systems*, JSV, Vol. 175, No. 2, pp. 159–170, 1994.

[11] **Balmes, E.**, *Orthogonal Maximum Sequence Sensor Placements Algorithms for modal tests, expansion and visibility.*, IMAC, January 2005.

[12] **Lalanne, M.** and **Ferraris, G.**, Rotordynamics prediction in Engineering, Wiley, 1998.

[13] **Genta, G.**, Dynamics of Rotating Systems., Springer, New-York, 2005.